International Journal of Nanomedicine

Dovepress
Taylor & Francis Group

Open Access Full Text Article

ORIGINAL RESEARCH

Polysarcosine-Functionalized Graphene Oxide Improves Biological Safety and Enhances Chemo-Photothermal Therapy Synergistic Anticancer Effect

Weiwei Ma[1,*], Yan Zhang[2,*], Xuejing Zhai[1], Qian Qu[1], Xueying Guo[1], Sen Zhang[1], Ruiyao Hou[1], Ping Lu[2], Yanyan Yin[1]

[1]College of Pharmacy, Xinxiang Medical University, Xinxiang, People's Republic of China; [2]Department of Oncology, The First Affiliated Hospital of Xinxiang Medical University, Xinxiang, People's Republic of China

*These authors contributed equally to this work

Correspondence: Weiwei Ma, College of Pharmacy, Xinxiang Medical University, Xinxiang, 453003, People's Republic of China, Tel/Fax +86 0373 3029879, Email 081011@xxmu.edu.cn; Yanyan Yin, Email 105772801@qq.com

Background: Graphene oxide (GO) has high drug-loading capacity and good photothermal property. However, the limited stability and poor biocompatibility of GO hindered its application as drug delivery carrier for future nanomedicine.

Methods: In this study, a new strategy of using chemical conjugation on GO with polypeptide was adopted. A novel Biotin grafted polysarcosine polymers (B-PSar) modified graphene oxide derivative (B-PSar-GO) was successfully synthesized and utilized as a carrier to develop a new drug delivery system for targeted chemo-photothermal cancer therapy. In vitro and in vivo experiments evaluated the system's biosafety and antitumor efficacy.

Results: With the B-PSar protection, the B-PSar-GO showed excellent biological safety with the average size of 268.2±8.4 nm. Stability experiments displayed B-PSar-GO was extremely stable. The anti-cancer drug doxorubicin (DOX) was loaded on B-PSar-GO through π–π interactions and hydrophobic interactions, B-PSar-GO@DOX achieved a maximum loading capacity of 25.5%. In addition, B-PSar-GO@DOX exhibited NIR/pH dual-responsive DOX release characteristics, ensuring sustained drug release to tumor tissues triggered by NIR laser irradiation and acidic tumor microenvironment. Based on the excellent photothermal conversion efficiency of GO, B-PSar-GO@DOX showed excellent chemo-photothermal synergistic tumor inhibition both in vitro and in vivo under NIR irradiation.

Conclusion: The novel nano-drug delivery system B-PSar-GO@DOX developed in this paper offers a promising platform for chemo-photothermal synergistic cancer treatment.

Keywords: polysarcosine, graphene oxide, photothermal-chemotherapy, NIR/pH dual-responsive, drug delivery system

Introduction

Due to the high incidence rate and death rate of cancer, cancer treatment has always been one of the hot spots in the scientific community.[1] In clinics, the treatment of cancer usually includes surgery, chemotherapy, radiotherapy, hormonal treatments and targeted biological therapies.[2] However, these traditional therapies suffer from issues such as high trauma, low targeting, and susceptibility to drug resistance, which severely limit their anti-tumor efficacy and prognosis.[3] In recent years, photothermal therapy (PTT) has become a promising alternative or supplement to traditional cancer treatment due to its low invasiveness and toxic side effects, short acting time, and low incidence of complications.[4,5] Photothermal therapy refers to the therapeutic method using materials that absorb optical energy and convert it into thermal energy, thus, inducing cancer cell apoptosis or necrosis with hyperthermia. It has been used in clinical practice to

Received: 7 July 2025
Accepted: 4 December 2025
Published: 19 December 2025

ablate malignancies including melanoma, breast cancer, head and neck cancer, and pancreatic cancer.[6] This strategy avoids severe infection-related syndromes that are usually encountered after surgery and averts the side effects from chemotherapy drugs.[7] Increasing research studies have shown that combining photothermal therapy with chemotherapy holds significant potential in cancer treatment due to controlled drug release, minimal side effects, and improved therapeutic effectiveness.[8,9]

Graphene has a two-dimensional planar structure and was first discovered in 2004.[10] The isolation of graphene and in-depth research on its unique properties have promoted significant progress in the application of its derivative graphene oxide (GO) in different industries. Since then, graphene oxide and its composite materials have received widespread attention in biological fields such as gene and drug delivery, intracellular tracking, etc. due to their good dispersibility, high drug loading rate, high near-infrared absorption rate and large surface area.[11–14] However, one of the main issues with graphene oxide based nanomaterials in biomedical applications is the inherent toxicity and health risks of the compound, which mainly depend on factors such as its size, number of layers, surface charge, shape, surface functional groups, and particle properties.[15] GO has many oxygen moieties, such as epoxy and hydroxyl groups on the top and bottom of each sheet, as well as carbonyl, carboxyl, hydroxyl, lactone, and phenolic structures at the edges of the flakes.[16,17] These functional groups enhance the dispersibility of graphene oxide in water.

Proper functionalization of graphene oxide can mitigate much of its toxic effects.[18] Numerous compounds have been surface-functionalized on graphene oxide to enhance its biological applications and mitigate cell toxicity.[19–22] Polymer coating is a way to functionalize the surface of graphene oxide, including chitosan (CS),[23] polyethylene glycol (PEG),[24] polyethylenimine (PEI),[25] polyacrylic acid (PAA),[26] and polyvinyl alcohol (PVA).[27]

Polypeptide-based drug delivery system exhibited outstanding biodegradability and biocompatibility, prolonging their circulation time in vivo.[28,29] Polysarcosine (PSar), a polypeptoid derived from N-methylated glycine, has properties similar to polyethylene glycol, as it has high water solubility and exhibits hydrogen bond acceptor properties due to methylation of amide nitrogen atoms.[30–33] Furthermore, it is a non-ionic zero charge polypeptide with non immunogenicity and low cytotoxicity. Recently, many studies reported that PSar have good applications in biomedical fields.[34] Zhu et al[32] reported polysarcosine coating gold nanorods for near-infrared photothermal tumor therapy. Wilhelmy et al[35] designed polysarcosine-Functionalized mRNA Lipid Nanoparticles Tailored for Immunotherapy.

Herein, we reported a new drug delivery nanoplatform based on polysarcosine-coated graphene oxide for synergistic chemotherapy-PTT therapy against tumors. As shown in Scheme 1, GO was modified with polysarcosine and active cancer targeting biotin to construct a novel nano drug carrier B-PSar-GO. Then, DOX was anchored on the GO surface by π-π stacking and hydrophobic interaction to obtain multifunctional B-PSar-GO@DOX nanoplatform. After modification with polysarcosine, the biocompatibility and physiological stability of nanoparticles were significantly improved. Under near-infrared (NIR) light irradiation, the local thermal therapy generated by graphene oxide with enhanced photothermal efficiency can also accelerate B-PSar-GO@DOX the release of DOX in the tumor enables the combination of enhanced chemotherapy and tumor PTT.

Materials and Methods

Materials

Z-sarcosine, sulfoxide chloride, N-Boc-ethylenediamine, N,N-diisopropylethylamine (DIPEA), (1-cyano-2-ethoxy-2-oxoethylidenaminooxy) dimethylamino-morpholino-carbenium hexafluorophosphate (COMU), Biotin, DOX, Graphene oxide were purchased from Aladdin Reagent Co. Ltd. (Shanghai, People's Republic of China). 3-(4,5-dimethylthiazol-2-yl)-2,5-diphenyltetrazolium bromide (MTT), 4,6-diamino-2-phenylindole (DAPI) were purchased from Beyotime Biotechnology Co., Ltd. (Shanghai, China). Other reagents were bought from Tianjin Beichen Chemical Reagent Co., Ltd (Tianjin, People's Republic of China). All the chemical reagents were analytical grade without any further purification.

The 4T1 mouse breast cancer cells and HEK293 cells were purchased from iCell Bioscience Inc (Shanghai, China). The use of the cell lines was approved by the ethics committee of Xinxiang Medical University (20240192). The cells were cultured at 37°C and 5% CO_2 in high-glucose Dulbecco's Modified Eagle Medium (DMEM) supplemented with

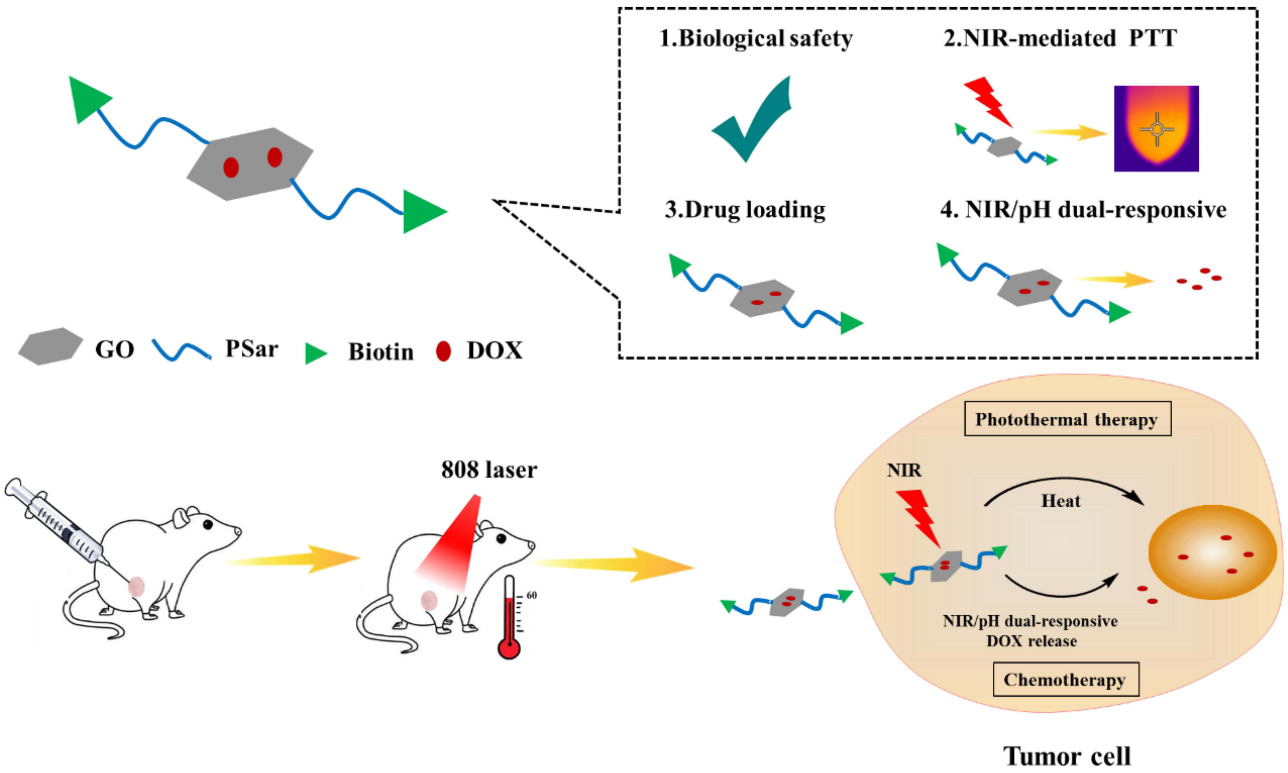

Scheme 1 Schematic illustration of the preparation B-PSar-GO@DOX and its synergistic Chemo-Photothermal therapy against tumor.

10% fetal bovine serum (FBS), 1% penicillin, and 1% streptomycin. Specific pathogen-free Kunming mice were obtained from the Laboratory Animal Center of Xinxiang Medical University. Balb/c mice were purchased from Henan Skobes Biotechnology Co., Ltd.

Synthesis of Biotin-Polysarcosine-Graphene Oxide (B-PSar-GO)

Synthesis of Sarcosine N-Carboxyanhydride (Sar-NCA)

To obtain Sar-NCA (sarcosine n-carboxylic anhydride), 2.5 g (11.2 mmol) Z-sarcosine was put into 25 mL round-bottom flask, 2.5 mL sulfoxide chloride was added, and then the mixture stirred 60°C for 20 min. Then the reaction liquid was poured into 60 mL of petroleum ether, and the reaction system quickly precipitated light yellow flocculent precipitate. Precipitates were collected by filtration and dried in vacuum for 4 h. Following, a small amount of hot ethyl acetate was added to the crude product and filtered, the filtrate was poured into 100 mL of cold petroleum ether, the precipitation was filtered and dried in vacuum. Repeat the above purification steps three times, the Sar-NCA was obtained as a white powder. ^{1}H NMR (400 MHz, $CDCl_3$) δ [ppm] = 4.13 (s, 2H, -CH_2-CO-), 2.99 (s, 3H, -CH_3).

Synthesis of Boc-Polysarcosine (Boc-PSar)

Sar-NCA 0.97 g (0.8245 g, 7.16 mmol) and N-Boc-ethylenediamine 41 μL (0.26 mmol) were added into a round-bottled flask with 10 mL of dried DMF under argon atmosphere. The mixture was stirred at room temperature for 4 days. Then, the reaction solution was poured into 30 mL ethyl acetate and stirred vigorously for 5 min to obtain a white flocculent precipitate. The precipitation was washed twice in 10 mL ethyl acetate and dried in vacuum for 4 h to obtain the Boc-Polysarcosine. ^{1}H NMR (400 MHz, $CDCl_3$) δ [ppm] = 4.45–4.04 (br, 2n, CO-CH_2-N), 3.07–2.77 (br, 3n, -NCH_3-). The molecular weight of Boc-PSar (Mw = 2.13 kDa, PDI = 1.10) was calculated using the Gel Permeation Chromatography (GPC) method with Waters GPC 1515 (Waters, America) (column: Waters Styragel HT4).

https://doi.org/10.2147/IJN.S552175

Synthesis of Biotin-Polysarcosine-Graphene Oxide (B-PSar-GO)

Take 100 mg Boc-Polysarcosine and 50 mg graphene oxide, COMU (100 mg) and DIPEA (50 mg) into a round-bottom flask, added 3 mL DMF to dissolve the reaction mixture, stirred at room temperature for 9 h. Then the reaction solution was transferred to 8000–14000 Da dialysis bag, and deionized water was used as dialysate for dialysis at room temperature for 12 h. After dialysis, the liquid in the dialysis bag was freeze-dried, which was Boc-PSar-GO. Then the obtained Boc-PSar-GO was dissolved in methanol, adding 50%TFA (methanol: 50%TFA = 3:1), and stirred at room temperature for 3 hours. After the completion of the reaction, the mixture was purified by dialysis (molecular cutoff, 8000–14000) against deionized water for 1 days and freeze-dried to give PSar-GO. Next, PSar-GO (140 mg), Biotin (50 mg), COMU (87 mg) and DIPEA (25 mg) dissolved in an appropriate amount of anhydrous DMF and then stirred at room temperature for 3 h. Then, the mixture was purified by dialysis (molecular cutoff, 8000–14000) against deionized water for 1 days. The dialysate was freeze-dried to give B-PSar-GO.

Characterization of B-PSar-GO

The chemical structure B-PSar-GO were confirmed through FTIR and ^{1}H NMR. ^{1}H NMR spectra were recorded on Bruker Avance/400 (1H: 400 MHz at 25°C). For FTIR spectra, the samples were illustrated with KBr mixing powder at 1% (w/w) and pressed to obtain self-supporting disks. IR spectra were recorded from 500 to 4000 cm $^{-1}$ at room temperature. The hydrodynamic diameter and zeta potential of the B-PSar-GO were analyzed by using a ZS-90 particle size analyzer (Malvern, England). Thermogravimetric Analysis (TGA) were recorded using TGA instrument (TGA/DSC 2, STAR system, MettlerToledo, Switzerland) under nitrogen atmosphere from room temperature to 600°C. The micromorphology of B-PSar-GO was observed and photographed using an H7500 transmission electron microscope (TEM, Hitachi, Japan). The stability of B-PSar-GO was investigated in vitro. Briefly, the B-PSar-GO suspensions (1.0 mg/mL) were stored at room temperatures, at specific time intervals, and the size distribution and PDI were monitored by using a ZS-90 particle size analyzer (Malvern, England).

Photothermal Effect of B-PSar-GO

The photothermal effect of B-PSar-GO was analyzed using an external 0–18 W adjustable laser (808 nm, Beijing Hi-Tech Optoelectronic Co., China). B-PSar-GO with different concentration (0.1, 0.5 and 1.0 mg/mL in PBS) and PBS were treated with 808 nm laser irradiation (2 W/cm^2) for 5 min. The temperature of solutions and NIR thermal images was recorded by a thermal camera (FLIR E60, Estonia) every 30 seconds. The photothermal effects of different laser powers (0.5, 1.0, 1.5, and 2.0 W/cm^2) were investigated in the same way. In addition, to assess the photothermal stability of B-PSar-GO, four laser "on-off" cycles were performed. Briefly, after irradiating B-PSar-GO for 5 min at different concentration, the laser was turned off for cooling. Subsequently, all samples were irradiated again, and this process was repeated four times.

Preparation and Characterization of B-PSar-GO@DOX

To load the DOX onto B-PSar-GO, B-PSar-GO (1.0 mg) dispersed in 4 mL DOX solution (0.1 mg/mL) and the solution was homogenized by ultrasound for 1 h in the dark. Then, the solution was stirred avoid light at room temperature to load the DOX onto the B-PSar-GO. After 24 h, the suspension was centrifuged at 10,000 rpm for 15 min to obtain the B-PSar-GO@DOX. The product was washed three times with water by centrifugation. The unloaded DOX was measured by UV-Vis spectrophotometer (483 nm), a standard DOX solution was prepared for quantitative analysis. The drug-loading efficiency (DLC) of DOX on B-PSar-GO and the encapsulation efficiency (EE) were measured as following equation:

DLC (%) = $M_1/(M_1+M_2) \times 100\%$

EE (%) = $M_1/M_3 \times 100\%$

Where M_1 represents the DOX loading amount. M_2 represents the mass of B-PSar-GO, M_3 represents the mass of DOX added at first.

B-PSar-GO@DOX nanoparticle was analysed by UV-vis and Fluorescence spectra.

In vitro Drug Release Assay

The in vitro drug release behavior of B-PSar-GO@DOX in a PBS (pH 5.8, 7.4) solution was measured by the dynamic dialysis (8000 Da) method. The dialysis samples were incubated at 37°C in the dark. At different time intervals (0.5, 2, 4, 6, 12, 24, 48 h), 2.0 mL solution was taken out, and 2 mL of PBS was supplemented. The amount of released DOX in the supernatant was measured using a UV-visible spectrophotometer (483 nm). Besides, in order to investigate the NIR stimuli-responsive behavior, the drug releasing performance of DOX from B-PSar-GO@DOX was researched with NIR (808 nm, 2.0 W/cm^2) light irradiation at predetermined times points for 10 min and supernatant was collected for UV-Vis spectrophotometric analysis. The percentage of drug releasing was calculated by the following:

The percentage of drug released = $M_{released}/M_{loaded} \times 100\%$

Where, $M_{released}$ represents the DOX release amount, and M_{loaded} represents the DOX loading amount, respectively.

In vitro Hemolytic Assay

The blood compatibility of B-PSar-GO was assessed by hemolysis test. 2.0 mL fresh mice blood was collected and centrifuged to obtain erythrocytes, then the erythrocytes diluted with normal saline (NS) to make 2% erythrocyte suspension. B-PSar-GO with different concentrations were introduced to the erythrocyte suspensions and incubated at 37°C for 4 h, sterilized water and normal saline were used as positive and negative controls, respectively. After image acquisition, all the samples were centrifugated at 1500 rpm for 10 min. Finally, the absorbance of supernatant was measured at 545 nm by the Molecular Devices Spectra Max i3microplate reader. The hemolysis rates were calculated according to the following equation.

Hemolysis rate = (ODsample–OD_0) / (OD_{100}–OD_0)

Where, ODsample represent the supernatant absorbance of the sample, OD_0 represent the supernatant absorbance of a solution of 0% hemolysis, OD_{100} represent the supernatant absorbance of a solution of 100% hemolysis, respectively.

In vitro Cellular Uptake Assay

4T1 cells (5×10^4 cells per well) were seeded into a 24-well plate and incubated overnight to attaching to the wall. Then, the medium was discarded, and the cells were incubated with fresh medium containing free DOX and B-PSar-GO @DOX, respectively. After incubating for 2 h, the cell nuclei were stained with DAPI (2 μg/mL), then the cells were washed with PBS. The fluorescence photograph of 4T1 cells were taken using a fluorescence microscope (excitation wavelength: 480 nm, emission wavelength: 590 nm).

Cytotoxicity Assay in vitro

The in vitro cytotoxicity of B-PSar-GO was investigated by using HEK293 cells. In brief, HEK293 cells were seed into 96-well plates at a density of 10000 cells/well and incubated at 37°C for 24 h. Then the cells were treated with 100 μL fresh medium containing PBS and B-PSar-GO at the different concentration (0.5, 5, 50, 250 μg/mL) for 24 h. After that, the old medium was replaced by fresh culture medium containing MTT. The cells incubated in the dark for another 4 h. Then 150 μL DMSO were added into above wells to dissolve the formazan crystals. The optical density values of cells in each well at 490 nm were detected with a microplate reader (Thermo Scientific Multiskan Go, USA).

In addition, the in vitro tumor cell killing efficiency was evaluated using the same method with 4T1 cells as models. The in vitro 4T1 cell viabilities of B-PSar-GO, B-PSar-GO+NIR, DOX, B-PSar-GO@DOX, B-PSar-GO@DOX+NIR were evaluated using the MTT method described above. The applied concentrations of DOX ranged from 0.5 to 20 μg/mL. The experimental groups requiring NIR treatment were stimulated with an 808 nm laser (1.0 W/cm^2) for 10 min.

In vivo Biosafety Evaluations

To investigation the in vivo biosafety of B-PSar-GO, 12 Kunming mice (6–7 weeks) were randomly divided into two groups, ie normal saline (NS), B-PSar-GO, respectively. The mice were treated with (i) normal saline, (ii) B-PSar-GO (2.5 mg/kg) every 3 days by tail vein injection. During the experiment, the mice were observed daily for mortality, dietary habits, changes in appearance, behavioral abnormalities and toxicity. The body weights were recorded every 3

days. After 21 days of experimental observation, the mice were sacrificed, and blood sample and all main organ tissues were collected. Blood indicators were monitored using XS-500i fully automated hematology analyzer (Sysmex, Japan) and biochemical analyzer (Olympus AU400, Japan), respectively. The organ weights were recorded and the organ coefficients were calculated according to the following equation: Organ coefficient (%) = (Organ weight/Mouse body weight) × 100. In addition, the H&E staining experiment was conducted to investigate pathological changes caused by B-PSar-GO.

In vivo Antitumor Effects

4T1 tumor-bearing BALB/c mice was established by injecting of 4T1 cell suspension (1×10^4 cells per mice) in the right flanks of the mice. When the tumor volume of reached 60–80 mm^3 ($V = (L \times W^2) / 2$, where L and W represent the major and minor axes of tumor tissue), the mice were randomly divided into four groups: normal saline (NS), DOX, B-PSar-GO@DOX, B-PSar-GO@DOX+NIR. The DOX dosage was fixed at 5.0 mg/kg, and all the solution were injected every 3 days by peritumoral injection. In the near-infrared laser treatment group, the tumors were irradiated with an NIR laser (808 nm, 1.0 W/cm^2) for 10 min. The tumor volumes and body weights were measured every three days. After 18 days treatment, the mice were necropsied, the tumors were collected. The tumors were fixed with 4% paraformaldehyde. H&E and TUNEL staining was used on tumor for histological analysis.

Statistical Analysis

The results of this study were presented as mean ± SD. Statistical analysis was performed using GraphPad Prism 7.0 software (GraphPad Software, Inc., La Jolla, CA). An unpaired Student's *t*-test (two-tailed) was employed to ascertain differences between the two means. For multiple group comparisons, a two-way ANOVA was conducted, followed by a Tukey's multiple comparisons test. $P < 0.05$ was deemed statistically significant.

Results and Discussion

Synthesis of B-PSar-GO Conjugate

B-PSar-GO conjugate was synthesized according to the Scheme 2. Sarcosine-N-carboxy anhydride (Sar-NCA) was prepared from Z-Sar-OH following the reported methods.[36] Polymerization was carried out using Sar-NCA in dry DMF with N-Boc-ethylenediamine as the initiator. Then the carboxyl group of GO and the amino group on Boc-PSar were linked together through amidation reaction. After removing the protective group, biotin was attached to PSar-GO by amidation reaction.

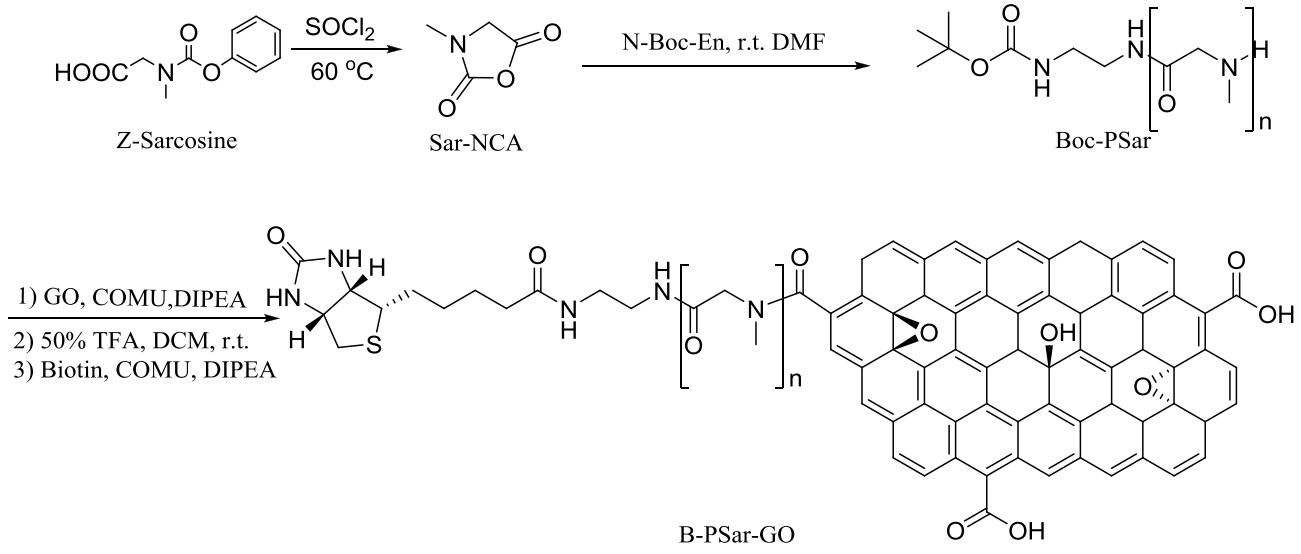

Scheme 2 Synthesis scheme of B-PSar-GO.

Characterization of B-PSar-GO

In the ^{1}H NMR spectroscopy (Figure S1-S2), the proton signal of the methylene group on the backbone of sarcosine appears in 4.04–4.45 ppm. The proton signal of methyl groups of Sar residues appears in 2.77–3.05 ppm. The ring-opening polymerization of Sar-NCA was initiated using N-Boc-ethylenediamine, after the polymerization, the signature of Sar-NCA FTIR peaks at 1765 and 1851 cm^{-1} ascribed to the C=O stretching vibration disappeared (Figure 1A). [35] In addition, the stretching vibration peak of C=O of the amide bond at 1663 cm^{-1} indicated successful synthesis of polysarcosine.

Furthermore, compared to the spectrum of GO (Figure 1B), FTIR spectra of PSar-GO had obvious C-H (1406 cm^{-1}), C-N (1109 cm^{-1}), and N-H (842 cm^{-1}) vibration peaks of PSar block, indicating PSar was attached to GO. The FTIR spectral analysis of B-PSar-GO indicates the presence of a new characteristic peak at 1631 cm^{-1}, corresponding to the extension of the amide carbonyl group from the newly formed amide functional group (Biotin), which indicated B-PSar-GO was successfully prepared.

In addition, thermogravimetric analysis (TGA) was conducted to further prove the successful preparation of B-PSar-GO (Figure 1C). From TGA analysis, the slight mass loss of GO at <100°C might because of the evaporation of residual water, the mass loss declined sharply at 200°C might be attributed to the hydroxyl, carboxyl and epoxy on GO gradually decomposed. For the curve of B-PSar-GO, similar to GO, the first mass loss was observed <100°C because of the evaporation of water molecules, the second step about 200°C due to the hydroxyl, carboxyl and epoxy gradually decompose, then the curve tends to be gentle until the temperature rose to about 350°C, there was a clear turn might correlate to the decomposition of functional groups on GO. All the above results showed the successful synthesis of B-PSar-GO.

As shown in Table 1, graphene oxide had electronegativity with a surface potential of −29 ± 2.54 mV. This is mainly due to the presence of oxygen on the surface of graphene oxide functional groups (such as carboxyl, epoxy groups). After the introduction of polypeptide on GO, the zeta potential increased to −7.6±0.08 mV. Moreover, an increase in the

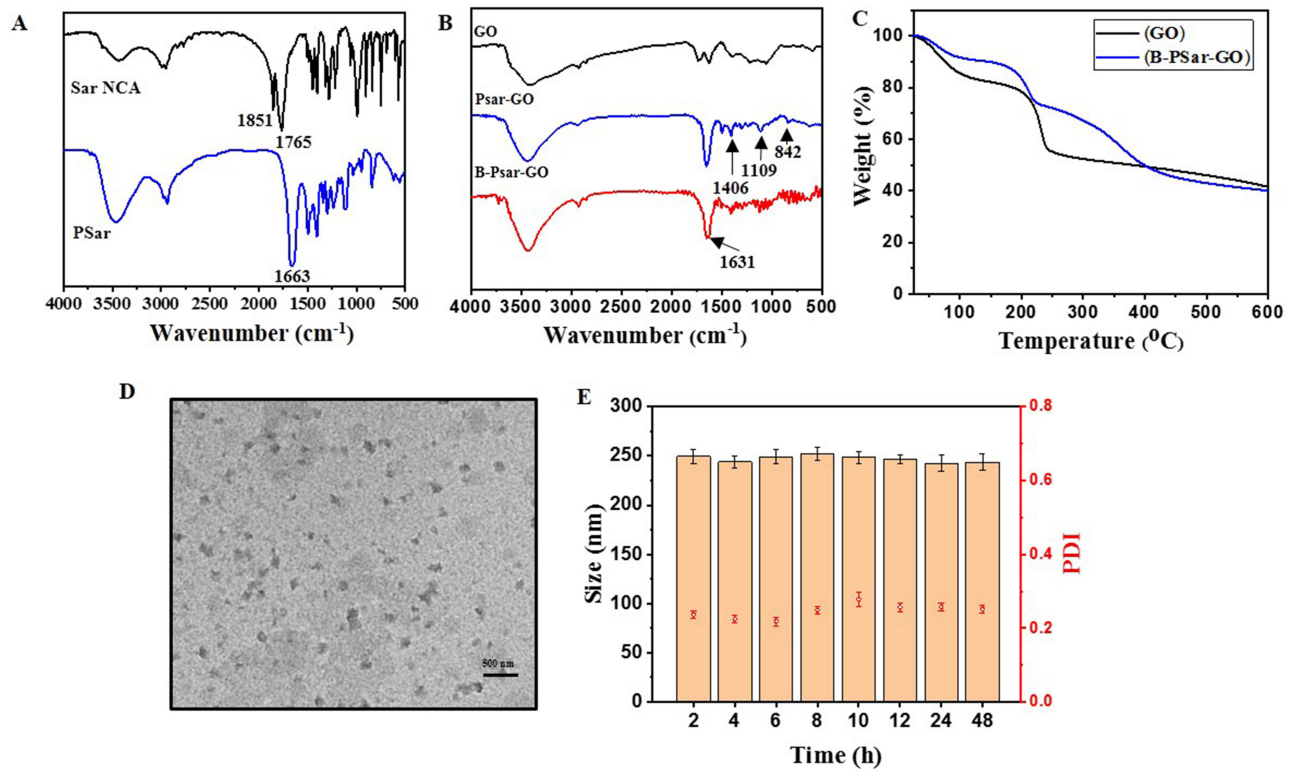

Figure 1 FTIR spectra of Sar NCA and PSar (**A**). FTIR spectra of GO, PSar-GO, B-PSar-GO (**B**). TGA curves of GO, B-PSar-GO (**C**). TEM images of B-PSar-GO (**D**). Stabilities of B-PSar-GO (1 mg/mL) at room temperature (**E**).

https://doi.org/10.2147/IJN.S552175

Table 1 Particle Size and Zeta Potential of GO and B-PSar-GO

Sample	Size (nm)	Polydispersion Index	Zeta Potential
GO	245.1±6.8	0.225±0.013	−29±2.54
B-PSar-GO	268.2±8.4	0.240±0.011	−7.6±0.08

particle size of the nanoparticles was observed following the addition of B-PSar (Figure S3–4). The particle size of graphene oxide is 245.1±6.8 nm, while the particle size of B-PSar-GO increases to 268.2±8.4 nm. Then TEM was employed to examine the morphology of the B-PSar-GO nanoparticles. In TEM image showed B-PSar-GO presented as a sheet structure and uniform in size with an average particle size of 250 nm (Figure 1D). In stability experiments, after being stored at room temperature for 48 h, the particle size of B-PSar-GO did not change significantly, indicating that B-PSar-GO had good stability (Figure 1E).

Photothermal Effect of B-PSar-GO

To achieve the most effective chemo-photothermal treatment system, the NIR photothermal performance of B-PSar-GO was examined under different conditions. As observed in Figure 2A, with the irradiation of the NIR laser (808 nm, 2 W/cm^2) for 5 min, B-PSar-GO exhibited concentration dependent temperature changes. After irradiation, the temperature of B-PSar-GO at a concentration of 1 mg/mL increased by about 49.6°C, whereas that of PBS was only 1.2°C (Figure 2B). We further investigated the relationship between the laser power density with photothermal behavior, under 808 nm irradiation, the temperature increase was significantly correlated with laser power density, with higher laser densities resulting in greater temperature increases (Figure 2C). In addition, B-PSar-GO demonstrated stable photothermal conversion across four repeated irradiation cycles (Figure 2D). These results indicating B-PSar-GO exhibited superior photothermal conversion capabilities and have significant potential as a thermotherapeutic agent.

Characterization of B-PSar-GO@DOX

Many previous studies have shown that DOX can be loaded onto graphene surfaces by π-π stacking and hydrophobic effect. The size of B-PSar-GO@DOX increased to 273.4±0.023 after loading DOX. The DOX loaded onto PSar-GO was successfully verified by UV-vis spectrum and fluorescence spectra. From UV-vis analysis (Figure 2E), B-PSar-GO @DOX with an additional absorption peak at 485 nm arising from DOX confirmed the drug loading on B-PSar-GO @DOX. In addition, due to the DOX-GO interaction triggered by ground state electrons, the characteristic absorption peaks of both DOX and GO were redshifted. To verify this interaction, further research was conducted on the fluorescence properties. As shown in the Figure 2F the fluorescent intensity of DOX was diminished significantly. After DOX loading on B-PSar-GO, π-π stacking interaction between DOX and GO result in the efficient quenching of the fluorescence emissions.

The equation of the standard curve for DOX was established (Figure S5), the drug-loading rate was calculated to be 25.5% and the encapsulation efficiency was 73%.

In vitro Drug Release Assay

The release behavior of DOX from B-PSar-GO@DOX was investigated in PBS at pH 5.8 and pH 7.4 at 37°C. As shown in Figure 2G, the cumulative release of DOX was 32.4% at pH 5.8, compared to 19.6% at pH 7.4, indicating a slower release at the neutral condition. This is because under neutral conditions, the hydrogen-bonding interaction between DOX and GO is very strong. On the contrary, due to protonation, the interaction between the surface of graphene oxide and DOX reduced, and DOX on the surface of graphene oxide released faster in acidic environments. The pH responsive behavior was expected to target DOX delivery into tumors while protecting healthy tissues from damage. Moreover, considering the excellent photothermal conversion performance of B-PSar-GO, we examined the drug release behavior induced by NIR. The release rate of DOX induced by near-infrared laser increased sharply. The release rate was about twice as high as the sample without near-infrared laser irradiation. Therefore, the drug release performance of near-infrared stimulation indicated that the local

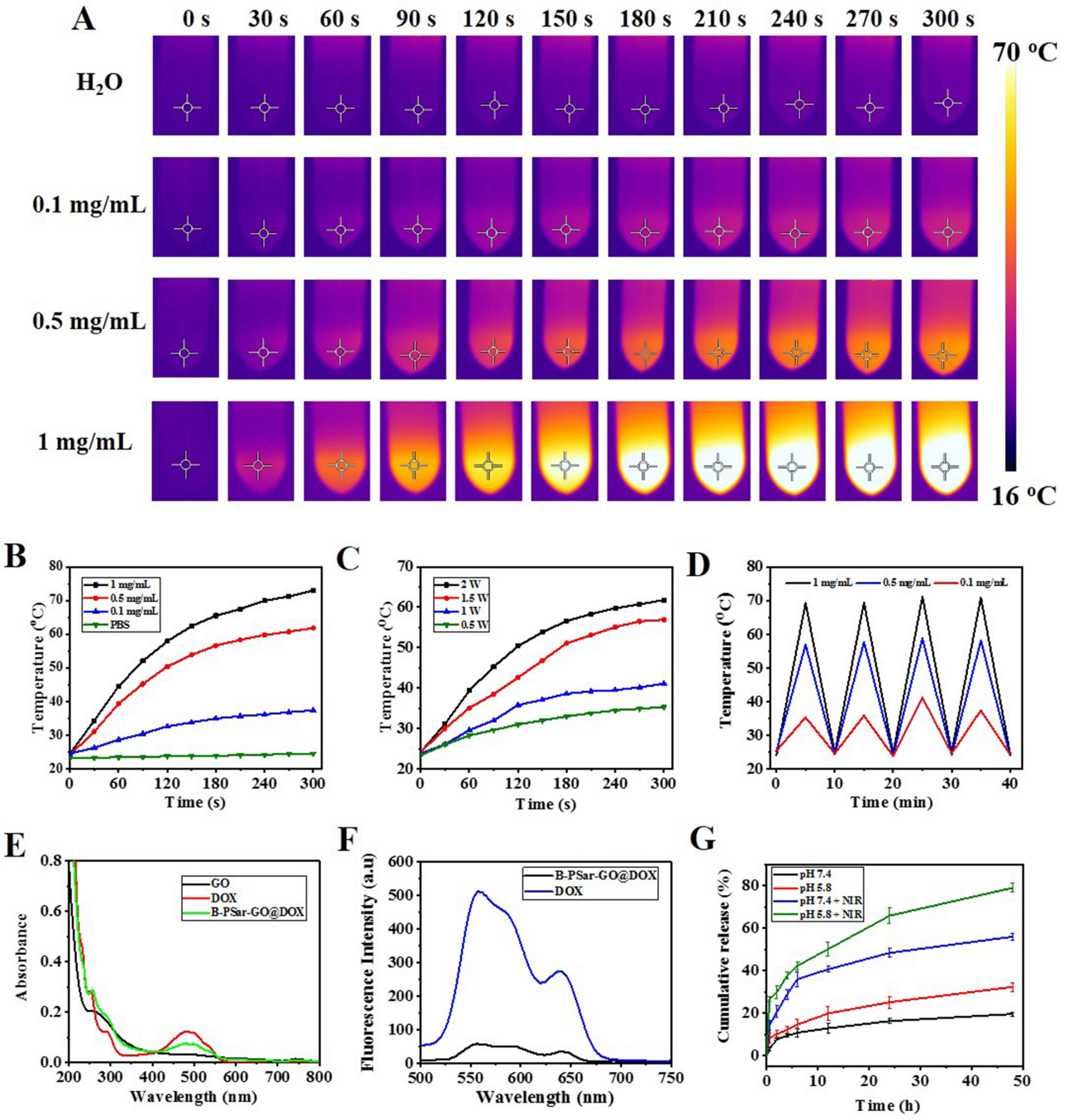

Figure 2 Thermographic images of B-PSar-GO under different sample concentrations (power density of the NIR laser was 808 nm, 2 W/cm^2) (**A**). Photothermal effects curves of different concentrations (0.1, 0.5, 1 mg/mL) of B-PSar-GO solution irradiated by NIR laser (808 nm, 2 W/cm^2) (**B**). Photothermal effects curves of 0.5 mg/mL B-PSar-GO solution under different 808 nm laser power densities (0.5, 1, 1.5, 2 W/cm^2) (**C**). Photothermal stability of different concentrations (0.1, 0.5, 1 mg/mL) of B-PSar-GO under four irradiation cycles (**D**). UV analysis of DOX, GO, DOX and B-PSar-GO@DOX (**E**). Fluorescence spectra of DOX, and B-PSar-GO@DOX (**F**). DOX release profiles in different conditions (**G**).

high temperature induced by photothermal effect can promote drug release at the tumor site, improve the efficacy of chemotherapy, and provide possibilities for the combined treatment of chemotherapy and photothermal therapy for tumors.

In vitro Hemolytic Assay

Good blood compatibility is crucial for nano drug carriers, as it was a prerequisite for ensuring their smooth entry into the human body and enabling them to function effectively. In the hemolysis experiment, physiological saline was the

https://doi.org/10.2147/IJN.S552175

negative control group (non hemolysis), and pure water was the positive control group (hemolysis). The hemolysis percentage and hemolysis image were shown in Figure 3A and B. Compared with the negative control group, there was no significant hemolysis within a certain concentration range (0.1–1 mg/mL). When the concentration of B-PSar-GO reached 1 mg/mL, the hemolysis rate was only 4.41%. These results indicate that B-PSar-GO had good blood compatibility and was suitable for in vivo administration.

In vitro Cellular Uptake Assay

The effective cellular uptake of nanoparticles was crucial for successful therapeutic outcomes. In the cellular uptake experiment, we chose 4T1 cells to study the cellular uptake behavior of B-PSar-GO@DOX in vitro. The blue fluorescence indicates the nuclei stained with DAPI, while the red fluorescence depicts the distribution of B-PSar-GO@DOX. After 2 hours of incubation, the cells showed strong red fluorescence, indicating that B-PSar-GO@DOX was absorbed into cells. Moreover, due to the targeting effect of biotin, the B-PSar-GO@DOX group showed more intense fluorescence compared to the free DOX group (Figure 3C). This result indicated that B-PSar-GO had excellent transport capacity and can effectively deliver chemotherapy drugs into tumor cells.

Cytotoxicity Assay in vitro

To elucidate the in vitro cytotoxicity of carrier materials and drug delivery systems, the MTT assays under different conditions were studied. It can be seen in Figure 3D and E, B-PSar-GO showed low cytotoxicity to HEK293 cells and 4T1 cells under different concentrations. Even at a concentration of 250 μg/mL, the cell viabilities were all more than 90%. These results indicated that the B-PSar-GO had good biocompatibility in vitro. However, upon irradiation of the cells with a NIR laser for four on/off cycles, there was a significant decrease in cell viability (Figure 3E). These findings demonstrated that B-PSar-GO possesses the capability to eliminate cells through its superior photothermal conversion effect. In addition, after loading DOX onto B-PSar-GO, the treatment effect of B-PSar-GO@DOX can be changed. The cell viability rates of B-PSar-GO@DOX and free DOX groups decreased, B-PSar-GO@DOX showed slightly less cytotoxicity than free DOX. More important, we found B-PSar-GO@DOX+NIR exhibited more significant cytotoxicity than B-PSar-GO@DOX and free DOX (Figure 3F), the IC_{50} values of B-PSar-GO@DOX+NIR and DOX were 0.36 ± 0.13 and 2.28 ± 0.4 μg/mL (Figure 3G), respectively. These results indicate that chemotherapy and photothermal can more effectively co-kill cancer cells.

In vivo Biosafety Evaluations

The in vivo safety assessment of B-PSar-GO was proceeded in this study. The temporal progression of body weights was illustrated in Figure 4A. In comparison to the control group (NS), mice in the experimental groups did not display significant fluctuations in body weight, indicating that the B-PSar-GO had no discernible effect on body weight. The organ coefficients, which were crucial indicators of the biotoxicity of biomaterials, were depicted in Figure 4B. All values were within the normal range and there was no significant difference between the normal saline group and B-PSar-GO groups, indicating B-PSar-GO have good biocompatibility.

To further evaluate the safety of B-PSar-GO, blood samples from mice in each experimental group were collected for hematological studies. The results of the blood routine examination and blood biochemistry analyses were shown in the Figure 4C and D. No statistically significant differences were observed in any blood routine indices and blood biochemical parameters between the control group and the B-PSar-GO group. These results indicated that B-PSar-GO did not cause toxicity to the blood system, confirming its biological safety.

To investigate the physiological and pathological effects of B-PSar-GO on mice, slices of mice main organs were taken for H&E staining experiments after 21 days of treatment. As shown in Figure 4E, after processing, no obvious pathological damage was found in any organs. Therefore, all the above experiments confirmed that B-PSar-GO was safe enough to be used as biomaterials.

In vivo Antitumor Effects

The in vivo anti-tumor efficacy of B-PSar-GO@DOX was assessed in BALB/c mice with 4T1 tumor xenografts following the experimental protocol shown in Figure 5A. The body weight and tumor volume of the mice were

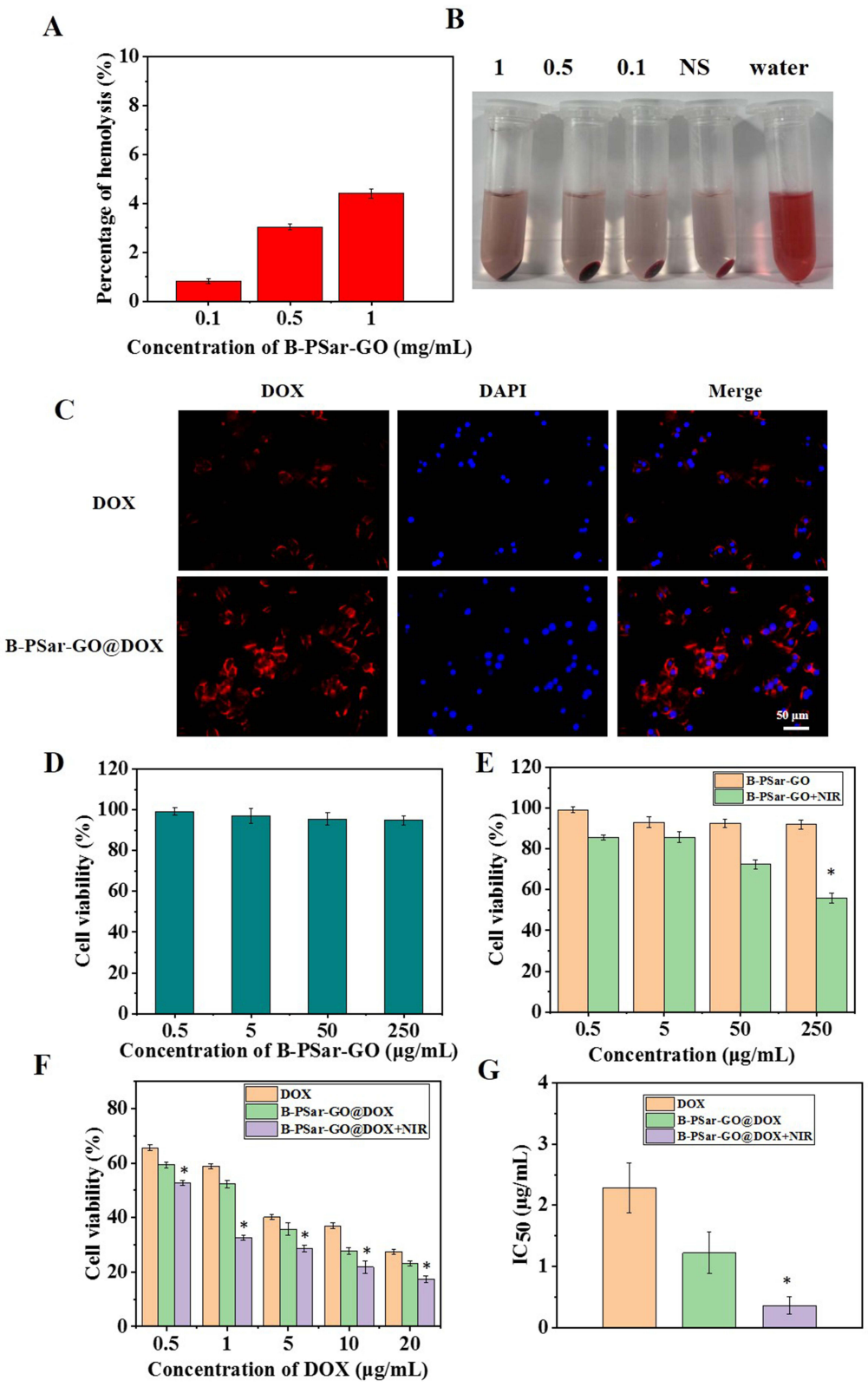

Figure 3 The percentage of hemolysis (**A**). Hemolysis test image (**B**). The cellular uptake of B-PSar-GO@DOX by 4T1 cells under the fluorescent inverted microscope (**C**). Cell viability of HEK293 treated B-PSar-GO (**D**). Cell viability of 4T1 treated with B-PSar-GO and B-PSar-GO+NIR (**E**). *p < 0.01 vs B-PSar-GO. Cell viability of 4T1 treated with DOX, B-PSar-GO@DOX and B-PSar-GO@DOX +NIR (**F**). *p < 0.01 vs DOX. IC_{50} values of DOX, B-PSar-GO@DOX and B-PSar-GO@DOX +NIR against 4T1 cells (**G**). *p < 0.01 vs DOX.

https://doi.org/10.2147/IJN.S552175

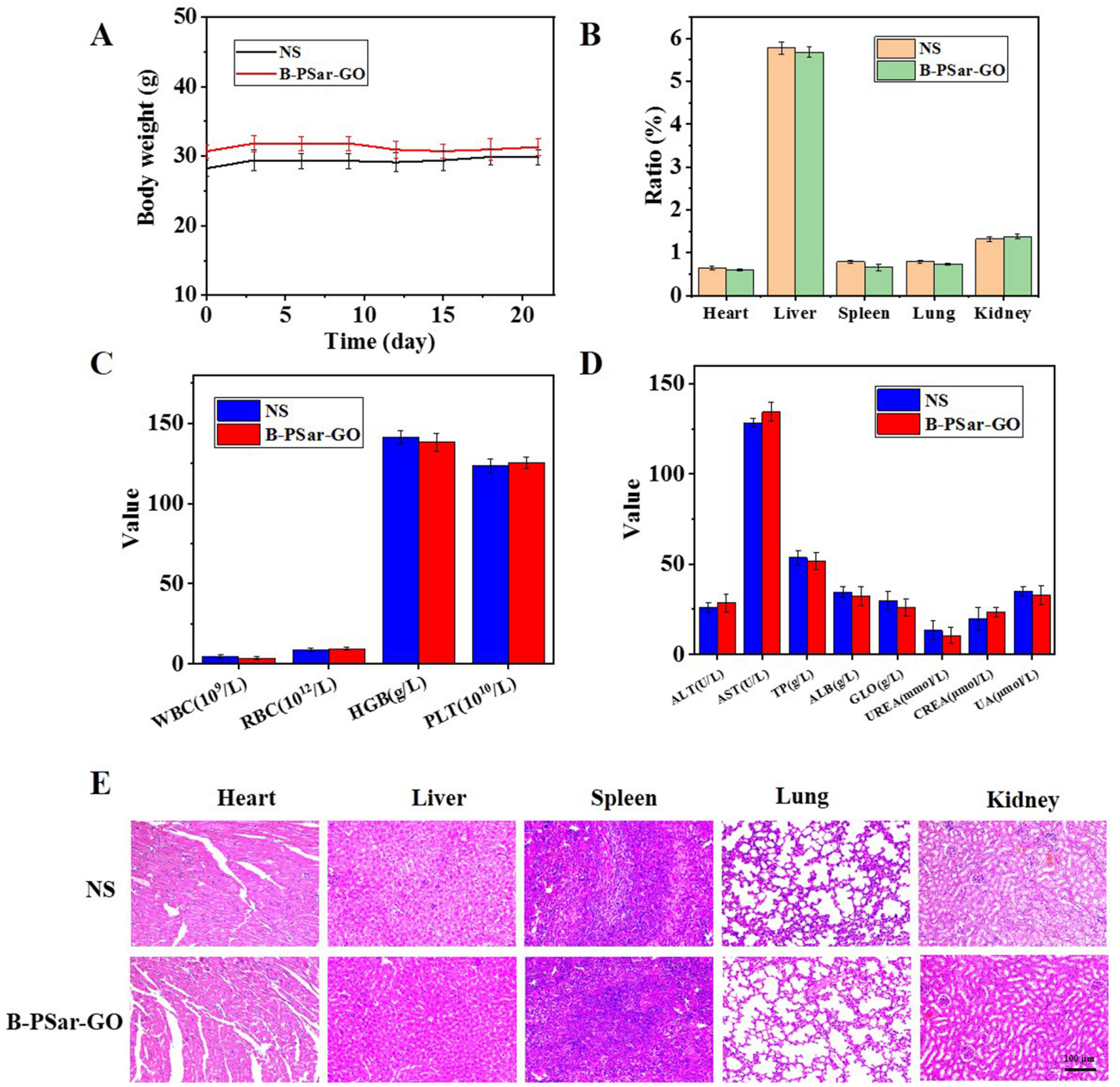

Figure 4 In vivo biosafety of B-PSar-GO. Body weights of treated mice (**A**). Organ coefficients of treated mice (**B**). Blood routine examination of treated mice (**C**). Blood biochemistry indexes of treated mice (**D**). H&E staining sections of main organs including heart, liver, spleen, lung, and kidney (**E**).

monitored. As shown in Figure 5B, the mice showed a gradual increase in body weight throughout the treatment process. Compared with the NS group, there was no significant change in the body weight in each experimental group, indicating the low biological toxicity of NPs. For tumor volume, after 18 days of treatment, the mice treated with NS had the largest tumors, with the relative tumor volume increasing by more than 6 times (Figure 5C). Compared to the NS groups, the B-PSar-GO@DOX group and chemotherapy groups (DOX) showed some tumor suppression, the tumor growth curves demonstrate a relatively slow progression. Furthermore, the B-PSar-GO@DOX+NIR treatment group displayed a superior anti-tumor effect compared to other groups. The reason for this excellent anti-tumor effect was the photo-thermal effect caused by graphene oxide (Figure 5D and E), which causing tumor cells to undergo reactions such as lysis and enzymatic degradation, ultimately leading to tumor cell death.

At the end of treatment, the tumor was removed (Figure 5F) and stained to continue verifying the therapeutic effect. H&E histological analysis (Figure 5G) showed that the morphology of tumor cells in the NS group remained normal, in the treatment

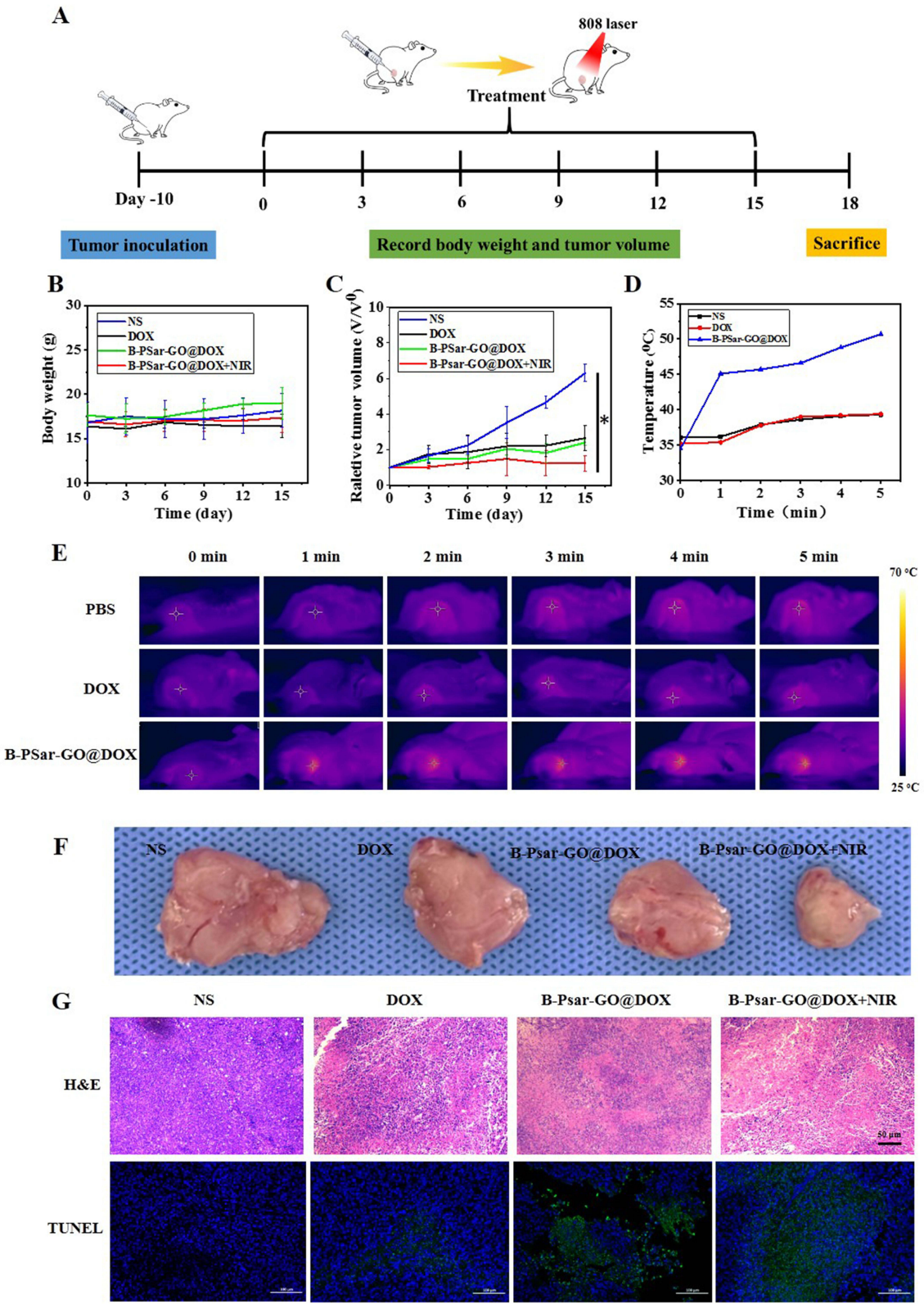

Figure 5 In vivo antitumor effects. Schematic illustration of the therapeutic protocol (**A**). Body weights of treated mice (**B**). Relative tumor growth curves (**C**). *p < 0.01 vs NS. Tumor temperature change curve (**D**). Infrared thermal imaging of tumor-carrying mice treated with NS, DOX, B-PSar-GO@DOX under 808 nm, 1 W/cm^2 laser irradiation. (**E**). Images of dissected tumors from mice after the treatment (**F**). H&E, TUNEL staining sections of tumor (**G**).

https://doi.org/10.2147/IJN.S552175

group of DOX and B-PSar-GO@DOX, cell destruction was limited, while the B-PSar-GO@DOX +NIR group exhibited severe cell damage. Moreover, immunofluorescent TUNEL staining was used to detect the degree of apoptosis of the tumor cells. The images (Figure 5G) showed that, relative to other groups, the B-PSar-GO@DOX +NIR group exhibited a higher number of TUNEL-positive cells, suggesting the combination of chemotherapy and PTT effectively induced tumor cell apoptosis. These results indicated that chemotherapy combined with photothermal therapy exhibits good anti-tumor effects.

Conclusion

In this study, a novel polyinosine-modified graphene oxide derivative (B-PSar-GO) was successfully synthesized and used as a carrier to construct a new drug delivery system B-PSar-GO@DOX for targeted chemo-photothermal therapy of cancer. The biosafety and photothermal conversion ability of B-PSar-GO was thoroughly investigated, and the results showed B-PSar-GO had excellent biological safety and superior NIR-controlled photothermal conversion ability. These characteristics supported its future as an effective carrier for drug delivery and photothermal therapy. After optimized DOX loading, the advantages of B-PSar-GO@DOX include high drug-loading efficiency, biocompatibility, robust photothermal properties and NIR/pH dual-responsive DOX release profiles. Studies conducted in vitro cell experiments showed that B-PSar-GO@DOX treated with near-infrared laser irradiation exhibited significant anti-tumor activity. Due to the high temperature of PTT causing local tumor thermal ablation, B-PSar-GO@DOX also showed effective chemotherapy and photothermal combined anti-tumor effects in vivo. In summary, B-PSar-GO@DOX hold great potential for enhancing chemo-photothermal therapy of cancer. In the future, more in-depth research on B-PSar-GO@DOX, such as long-term stability under different physiological conditions and immunogenicity, may pave the way for advanced anti-tumor treatments and applications.

Ethics Statement

All animal experiments were conducted in accordance with relevant laws, regulations, and the rules of the Animal Care and Use Committee of Xinxiang Medical University. All animal experiments were approved by the ethics committee of Xinxiang Medical University (20250072).

Acknowledgments

This work was supported by Henan Provincial Science and Technology Research Project (252102311228).

Disclosure

The authors report no conflicts of interest in this work.

References

1. Sung H, Ferlay J, Siegel RL, et al. Global cancer statistics 2020: GLOBOCAN estimatesof incidence and mortality worldwide for 36 cancers in 185 countries. *CA Cancer J Clin*. 2021;71:209–249. doi:10.3322/caac.21660
2. Miller KD, Nogueira L, Devasia T, et al. Cancer treatment and survivorship statistics, 2022. *CA Cancer J Clin*. 2022;72:409–436. doi:10.3322/caac.21731
3. Kaur R, Bhardwaj A, Gupta S. Cancer treatment therapies: traditional to modern approaches to combat cancers. *Mol Biol Rep*. 2023;50(11):9663–9676. doi:10.1007/s11033-023-08809-3
4. Li X, Lovell JF, Yoon J, Chen X. Clinical development and potential of photothermal and photodynamic therapies for cancer. *Nat Rev Clin Oncol*. 2020;17(11):657–674. doi:10.1038/s41571-020-0410-2
5. Zhao L, Wang X, Guan X, Zhang X, Zhang W, Ma J. Recent advances in selective photothermal therapy of tumor. *J Nanobiotechnol*. 2021;19(1):335. doi:10.1186/s12951-021-01080-3
6. Xiao F, Liu Y, Su Y, et al. Biodegradable Poly (amino acid)-Bismuth nanotheranostic agents for CT/MR imaging and photothermal-chemodynamic synergistic therapy. *Chem Bio Eng*. 2024;1(5):448–460. doi:10.1021/cbe.4c00078
7. Shang T, Yu X, Han S, Yang B. Nanomedicine-based tumor photothermal therapy synergized immunotherapy. *Biomater Sci*. 2020;8(19):5241–5259. doi:10.1039/D0BM01158D
8. Hao L, Song H, Zhan Z, Lv Y. Multifunctional reduced graphene oxide-based nanoplatform for synergistic targeted chemo-photothermal therapy. *ACS Appl Bio Mater*. 2020;3(8):5213–5222. doi:10.1021/acsabm.0c00614
9. Li X, Wang Y, Liu T, Wang Y, Zhang C, Xie B. Ultrasmall graphene oxide for combination of enhanced chemotherapy and photothermal therapy of breast cancer. *Colloids Surf B Biointerfaces*. 2023;225:113288. doi:10.1016/j.colsurfb.2023.113288
10. Novoselov KS, Geim AK, Morozov SV, et al. Electric field effect in atomically thin carbon films. *Science*. 2004;306(5696):666–669. doi:10.1126/science.1102896

11. Itoo AM, Vemula SL, Gupta MT, et al. Multifunctional graphene oxide nanoparticles for drug delivery in cancer. *J Control Release*. 2022;350:26–59. doi:10.1016/j.jconrel.2022.08.011
12. Jabłońska A, Jaworska A, Kasztelan M, Berbeć S, Pałys B. Graphene and graphene oxide applications for SERS sensing and imaging. *Curr Med Chem*. 2019;26(38):6878–6895. doi:10.2174/0929867325666181004152247
13. Mousavi SM, Hashemi SA, Ghasemi Y, Amani AM, Babapoor A, Arjmand O. Applications of graphene oxide in case of nanomedicines and nanocarriers for biomolecules: review study. *Drug Metab Rev*. 2019;51(1):12–41. doi:10.1080/03602532.2018.1522328
14. Báez DF. Graphene-based nanomaterials for photothermal therapy in cancer treatment. *Pharmaceutics*. 2023;15(9):2286. doi:10.3390/pharmaceutics15092286
15. Sattari S, Adeli M, Beyranvand S, Nemati M. Functionalized graphene platforms for anticancer drug delivery. *Int J Nanomed*. 2021;16:5955–5980. doi:10.2147/IJN.S249712
16. Piñeiro-García A, Semetey V. The "How" and "Where" behind the functionalization of graphene oxide by Thiol-ene "Click Chemistry". *Chemistry*. 2023;29(50):e202301604.
17. Salvio R, Krabbenborg S, Naber WJ, Velders AH, Reinhoudt DN, van der Wiel WG. The formation of large-area conducting graphene-like platelets. *Chemistry*. 2009;15(33):8235–8240. doi:10.1002/chem.200900661
18. Sharma H, Mondal S. Functionalized graphene oxide for chemotherapeutic drug delivery and cancer treatment: a promising material in nanomedicine. *Int J Mol Sci*. 2020;21(17):6280. doi:10.3390/ijms21176280
19. Dash BS, Lu YJ, Huang YS, Chen JP. Chitosan-coated magnetic graphene oxide for targeted delivery of doxorubicin as a nanomedicine approach to treat glioblastoma. *Int J Biol Macromol*. 2024;260:129401. doi:10.1016/j.ijbiomac.2024.129401
20. Shi Y, Xiong Z, Lu X, Yan X, Cai X, Xue W. Novel carboxymethyl chitosan-graphene oxide hybrid particles for drug delivery. *J Mater Sci Mater Med*. 2016;27(11):169. doi:10.1007/s10856-016-5774-6
21. Ma K, Li W, Zhu G, et al. PEGylated DOX-coated nano graphene oxide as pH-responsive multifunctional nanocarrier for targeted drug delivery. *J Drug Target*. 2021;29(8):884–891. doi:10.1080/1061186X.2021.1887200
22. Ghamkhari A, Abbaspour-Ravasjani S, Talebi M, Hamishehkar H, Hamblin MR. Development of a graphene oxide-poly lactide nanocomposite as a smart drug delivery system. *Int J Biol Macromol*. 2021;169:521–531. doi:10.1016/j.ijbiomac.2020.12.084
23. Rajput P, Khanchandani S. A review of chitosan-functionalized graphene oxide nanocomposites: a revolutionary drug delivery vehicle for cancer therapy. *Int J Biol Macromol*. 2025;311(Pt 4):143999. doi:10.1016/j.ijbiomac.2025.143999
24. Bao Y, Li H, He J, et al. Polyethylene glycol modified graphene oxide-silver nanoparticles nanocomposite as a novel antibacterial material with high stability and activity. *Colloids Surf B Biointerfaces*. 2023;229:113435. doi:10.1016/j.colsurfb.2023.113435
25. Mallick A, Nandi A, Basu S. Polyethylenimine coated graphene oxide nanoparticles for targeting mitochondria in cancer cells. *ACS Appl Bio Mater*. 2019;2(1):14–19. doi:10.1021/acsabm.8b00519
26. Nayl AEAA, El-Fakharany EM, Abd-Elhamid AI, et al. Fabrication and characterization of lactoperoxidase coated the modified graphene oxide-based nanocomposite for medical applications. *Int J Biol Macromol*. 2025;288:138597. doi:10.1016/j.ijbiomac.2024.138597
27. Garwal K, Rana A, Negi PB, et al. Designing magnetic graphene oxide-polymer nanocomposites for pH-responsive passive targeting of hydrophobic anticancer drug 5-fluorouracil for breast cancer therapy. *Int J Pharm*. 2025;682:125956. doi:10.1016/j.ijpharm.2025.125956
28. Wang X, Song Z, Wei S, et al. Polypeptide-based drug delivery systems for programmed release. *Biomaterials*. 2021;275:120913. doi:10.1016/j.biomaterials.2021.120913
29. Stepanova M, Nikiforov A, Tennikova T, Korzhikova-Vlakh E. Polypeptide-based systems: from synthesis to application in drug delivery. *Pharmaceutics*. 2023;15(11):2641. doi:10.3390/pharmaceutics15112641
30. Kabil MF, Azzazy HME, Nasr M. Recent progress on polySarcosine as an alternative to PEGylation: synthesis and biomedical applications. *Int J Pharm*. 2024;653:123871. doi:10.1016/j.ijpharm.2024.123871
31. Hu M, Taguchi K, Matsumoto K, Kobatake E, Ito Y, Ueda M. Polysarcosine-coated liposomes attenuating immune response induction and prolonging blood circulation. *J Colloid Interface Sci*. 2023;651:273–283. doi:10.1016/j.jcis.2023.07.149
32. Zhu H, Chen Y, Yan FJ, et al. Polysarcosine brush stabilized gold nanorods for in vivo near-infrared photothermal tumor therapy. *Acta Biomater*. 2017;50:534–545. doi:10.1016/j.actbio.2016.12.050
33. Birke A, Ling J, Barz M. Polysarcosine-containing copolymers: synthesis, characterization, self-assembly, and applications. *Prog Polym Sci*. 2018;81:163–208. doi:10.1016/j.progpolymsci.2018.01.002
34. Skoulas D, Stuettgen V, Gaul R, Cryan SA, Brayden DJ, Heise A. Amphiphilic star Polypept(o)ides as nanomeric vectors in mucosal drug delivery. *Biomacromolecules*. 2020;21(6):2455–2462. doi:10.1021/acs.biomac.0c00381
35. Wilhelmy C, Keil IS, Uebbing L, et al. Polysarcosine-functionalized mRNA lipid nanoparticles tailored for immunotherapy. *Pharmaceutics*. 2023;15(8):2068. doi:10.3390/pharmaceutics15082068
36. Sano K, Ohashi M, Kanazaki K, et al. Indocyanine green-labeled polysarcosine for in vivo photoacoustic tumor imaging. *Bioconjug Chem*. 2017;28(4):1024–1030. doi:10.1021/acs.bioconjchem.6b00715